Jurnal Rekayasa Mesin
p-ISSN: 1411-6863, e-ISSN: 2540-7678
Vol.21, No.2, August **2026**, p. 219-236

Numerical Analysis of Oblique Collision on Ship Bow Structure Using the Finite Element Method

Juan Abiegnail Sianipar[1*], Aldias Bahatmaka[1], Song Yeon Hee[2], Haris Nubli[3]
[1]Department of Mechanical Engineering, Universitas Negeri Semarang, Jl. Raya Banaran, Sekaran, Semarang City, Jawa Tengah, 50229, Indonesia
[2]Department of Naval Architecture and Marine Systems Engineering, Pukyong National University, Busan 48513, South Korea
[3]School of Engineering, University of Surrey, United Kingdom
*E-mail: juansianipar10@students.unnes.ac.id

Submitted: 06-07-2026; Accepted: 10-08-2026; Published: 31-08-2026

Abstract

Oblique bow collision is a complex maritime accident scenario, as the angled impact produces a non-uniform distribution of force and deformation, making the resulting damage substantially harder to predict than perpendicular collisions. Although numerous finite element studies have examined ship collision behavior, most have isolated a single parameter, leaving the combined effect of collision position and angle insufficiently characterized within a single validated numerical approach. This study addresses that gap by evaluating, for the first time within one validated numerical approach, the combined influence of collision position and angle on the structural response of a ferry-to-LPG carrier collision, using Explicit Dynamic Finite Element Method analysis in ANSYS Workbench 2024 R2 (LS-DYNA solver), with two collision positions (P1: main deck; P2: mid-body/bulbous bow) and three angles (90°, 120°, 135°) at 5 m/s across six scenarios, validated against experimental data with a crushing force error of 1.07%. Results show collision position more decisively affects structural resistance than angle, with P2 producing a peak force of 31.44 MN at 90°, over 60% higher than P1. Peak force and internal energy absorption were also found decoupled, with the highest energy absorbed at P2-120° (9.85 MJ) rather than the highest-force case, indicating that the P2-90° zone is structurally critical and warrants priority reinforcement, such as additional transverse framing or localized plate thickening. These findings support treating energy absorption as equally critical to peak force in ship collision safety assessment, in line with Sustainable Development Goal 9 (Industry, Innovation and Infrastructure), and future work is recommended to develop this numerical approach further through variations in collision velocity and distance.

Keywords: *finite element method; internal energy; crushing force; oblique collision; ship collision position*

Abstrak

Tabrakan miring pada haluan kapal merupakan skenario kecelakaan maritim yang kompleks, karena sudut tumbukan menghasilkan distribusi gaya dan deformasi yang tidak seragam, sehingga kerusakan yang timbul jauh lebih sulit diprediksi dibandingkan tabrakan tegak lurus. Meskipun berbagai studi elemen hingga telah mengkaji perilaku tabrakan kapal, sebagian besar hanya mengisolasi satu parameter, sehingga pengaruh gabungan antara posisi dan sudut tabrakan belum dikarakterisasi secara memadai dalam satu pendekatan numerik tervalidasi. Penelitian ini mengisi celah tersebut dengan mengevaluasi, untuk pertama kalinya dalam satu pendekatan numerik tervalidasi, pengaruh gabungan antara posisi dan sudut tabrakan terhadap respons struktural tabrakan antara kapal ferry dan LPG carrier, menggunakan metode elemen hingga dinamis eksplisit pada ANSYS Workbench 2024 R2 (solver LS-DYNA), dengan dua posisi tabrakan (P1: geladak utama; P2: bagian tengah badan/haluan bulbous) dan tiga sudut (90°, 120°, 135°) pada kecepatan 5 m/s dalam enam skenario, tervalidasi terhadap data eksperimental dengan error gaya hancur 1,07%. Hasil menunjukkan posisi tabrakan lebih dominan memengaruhi ketahanan struktural dibandingkan sudut, dengan P2 menghasilkan gaya puncak 31,44 MN pada 90°, lebih dari 60% lebih tinggi dibanding P1. Gaya puncak dan absorpsi energi internal juga ditemukan tidak berbanding lurus, dengan energi tertinggi terjadi pada P2-120° (9,85 MJ), bukan pada skenario bergaya tertinggi, mengindikasikan bahwa zona P2-90° bersifat kritis secara struktural dan memerlukan prioritas penguatan, seperti penambahan transverse framing atau penebalan pelat secara lokal. Temuan ini mendukung penempatan absorpsi energi setara pentingnya dengan gaya puncak dalam evaluasi keselamatan tabrakan kapal, sejalan dengan Tujuan Pembangunan Berkelanjutan (SDGs) ke-9 mengenai Industri, Inovasi, dan Infrastruktur, serta merekomendasikan penelitian lanjutan untuk mengembangkan pendekatan numerik ini melalui variasi kecepatan dan jarak tabrakan.

Kata kunci: metode elemen hingga; energi internal; gaya hancur; tabrakan miring; posisi tabrakan kapal

1. Introduction

Maritime transportation is essential for facilitating human mobility and the distribution of goods, especially in archipelagic nations such as Indonesia [1]. The high frequency of shipping activity elevates the risk of maritime accidents, including ship-to-ship collisions and impacts during berthing operations [1]. These incidents can result in structural damage to both the hull and bow, negatively impacting maritime safety, causing economic losses, and disrupting vessel operations [2]. Among the various collision scenarios, oblique bow collision is particularly complex because the impact occurs at a specific angle relative to the struck vessel's structure [3]. This scenario generates a non-uniform distribution of force and deformation, making the resulting damage mechanisms significantly more challenging to predict than those in perpendicular impact cases [4,5].

Understanding the structural response of ships under collision loading is fundamental to enhancing maritime safety and structural resilience [6]. In recent decades, advances in computational technology have facilitated the adoption of numerical methods as effective analytical tools for investigating ship collision phenomena [7–9]. The Finite Element Method (FEM) is one of the most widely used approaches because it can represent nonlinear structural behavior in detail, including stress distribution, plastic deformation, energy absorption, and material failure under impact [7]. This method enables the evaluation of structural responses under conditions that are challenging to replicate experimentally [10].

Numerous studies have used the Finite Element Method (FEM) to investigate the structural behavior and crashworthiness of ships under various collision scenarios. It has been demonstrated that the extent of structural damage is primarily determined by the kinematic interaction (including rebounding effects) between the striking and struck structures [11,12], although these studies were largely confined to a single, fixed collision configuration rather than a systematic variation of impact position and angle. Furthermore, detailed investigations into the progressive structural failure of side hulls during powered-bow collisions have provided critical insights into the rupture mechanisms of shell plating and internal transverse framing [13]. However, the analysis remained limited to a specific striking scenario without addressing how the collision position along the hull length influences the resulting failure pattern. Analysis of ship-side structures subjected to oblique bow collisions at different impact angles revealed a nonlinear reduction in peak crushing force as the impact angle increases [3], but this study isolated the angle parameter alone and did not examine its interaction with collision position. In a related study, evaluations of double-hull vessels have provided insights into their crashworthiness under both collision and grounding conditions [6], although the assessment focused on a single impact scenario rather than a parametric comparison across multiple positions and angles. To capture more complex dynamics, fluid–structure interaction has also been incorporated into the analysis of oblique collision scenarios [14] though this approach prioritized hydrodynamic coupling over a systematic structural parametric study. Additionally, specific parameters such as bow geometry and impact direction have been found to significantly affect the deformation pattern and failure mechanism [4,5,15], yet these studies generally varied one parameter at a time without jointly considering position and angle within a single validated framework. The reliability of numerical methods for predicting localized failure has also been successfully confirmed through the validation of Explicit Dynamic finite element models against field-measured stern damage [16], which strengthens confidence in the numerical approach but was not extended to a broader parametric investigation of oblique bow collisions. Collectively, these findings highlight that collision characteristics are critical in determining the extent of structural damage [17], underscoring the need for a more integrated evaluation framework.

However, research on oblique bow collisions has not fully addressed several important aspects [18]. Most prior studies have concentrated on specific collision conditions or isolated the influence of a single parameter, leaving the interaction effects between collision position and collision angle insufficiently characterized [5]. To date, no systematic study has evaluated the combined effects of collision positions (P1: main deck region or upper bow shoulder; P2: mid-body region or mid-bulbous bow) and collision angles (90°, 120°, 135°) within a single validated numerical framework at a velocity of 5 m/s for vessel configurations representative of Indonesian commercial shipping [1,19]. In summary, the research gap addressed in this study is the absence of a single validated numerical framework that jointly characterizes the combined effects of collision position and angle on the structural response of oblique ship bow collisions.

To address this research gap, the present study analyzes the structural response of a ship hull subjected to an oblique bow collision using Explicit Dynamic Finite Element Method (FEM) analysis in ANSYS Workbench 2024 R2 with the LS-DYNA solver at a constant initial velocity of 5 m/s. The main objective of this study is to evaluate the combined influence of collision position (P1, P2) and collision angle (90°, 120°, 135°) on three structural response quantities—directional displacement, crushing force, and internal energy absorption—of a ferry-to-LPG carrier collision, within a single validated numerical framework. These parameters are systematically varied across six scenarios, an integration that has not been previously established in the literature on oblique bow collision analysis. The novelty of this study lies in the structured parametric evaluation of three structural response quantities, directional displacement, crushing force, and internal energy, examined simultaneously under the combined variation of collision position and angle, thereby providing a more comprehensive characterization of the interaction effects that prior studies have largely treated in isolation. This unified framework is intended to inform the development of collision-resistant ship designs and to enhance maritime safety in Indonesian waters, in line with Sustainable Development Goal 9 (Industry, Innovation and Infrastructure), which emphasizes the development of resilient and reliable infrastructure, including maritime transportation systems that are vital to archipelagic nations such as Indonesia.

2. Material and Method

2.1. Ship Model and Material Properties

This study employs a ferry as the striking ship and an LPG carrier as the struck ship. The principal dimensions and characteristics of both vessels are taken from a numerical model [19], which provides a validated reference geometry for oblique collision analysis. The main specifications of each vessel are presented in Table 1.

Table 1. Principal Dimensions of the Ferry and the LPG Carrier [19]

Item	Ferry (Striking Ship)	LPG Carrier (Struck Ship)
Length Overall (LOA)	128.13 m	114.89 m
Ship Weight	5,757 t	3,607 t
Cargo Mass	1,132 t	2,148.6 t
Displacement	6,889 t	5,755.6 t
Mean Draught	5.28 m	4.71 m
Centre of Gravity Height	8.388 m	4.31 m
Longitudinal Centre of Gravity	61.082 m	63.74 m

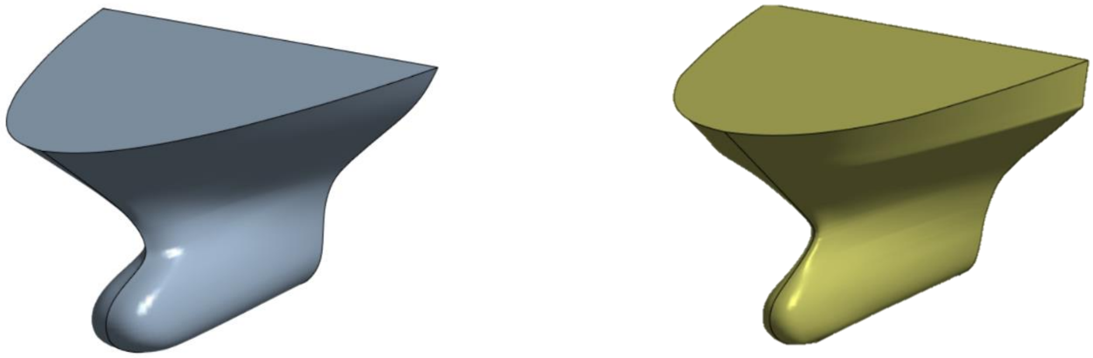

(a) **(b)**

Figure 1. Finite element models: (a) the ferry as the striking ship, (b) the LPG carrier as the struck ship

As shown in Figure 1, the striking ship (a) is modeled as a rigid body composed of structural steel, whereas the struck ship structure (b) is modeled using S235JR-EN10025 steel to represent the actual mechanical characteristics of shipbuilding steel. The material properties employed in the finite element model include density, elastic modulus, Poisson's ratio, yield stress, strength coefficient, strain-hardening exponent, and failure strain, as summarised in Table 2 [10,11].

Table 2. Material Properties of S235JR-EN10025 and Structural Steel [10,11]

Material	Property	Value
S235JR-EN10025	Density (*ρ*)	7800 kg/m³
	Young's Modulus (*E*)	210 GPa
	Poisson's Ratio (*ν*)	0.3
	Yield Stress (*σy*)	285 MPa
	Strength Coefficient (*K*)	740 MPa
	Strain-Hardening Exponent (*n*)	0.24
	Failure Strain (*εf*)	0.35
Structural Steel (Rigid Bow)	Density (*ρ*)	7850 kg/m³
	Young's Modulus (*E*)	200 GPa
	Poisson's Ratio (*ν*)	0.3

The geometric configuration and mass distribution of the vessels follow the approach commonly adopted in collision and grounding analyses, in which an adequate representation of the hull form is required to obtain accurate predictions of the structural response [19]. The use of S235JR-EN10025 steel has been reported to provide good agreement with penetration experiment results for small- to medium-sized ship structures [11]. Modeling the striking ship as a rigid body is a well-established practice in ship collision simulations, as it effectively represents the contact interaction at relatively low computational cost [17].

2.2. Collision Location and Impact Angle

The simulation parameters employed in this study are summarised in Table 3. Two collision locations are selected as the primary evaluation points: P1 and P2, as shown more clearly in Figure 2. P1 represents the upper bow region, or shoulder region, located in the vicinity of the forepeak tank, collision bulkhead, and forward deck supporting structures.

This region is critical for maintaining the watertight integrity of the vessel in the event of bow damage [2]. The relatively sharp geometric transition in the shoulder region may lead to higher stress concentrations during collision [3]. Structurally, this upper deck area features relatively thinner side-shell plating and limited transverse framing support.

P2, on the other hand, is located at the mid-bulbous bow region, adjacent to the lower forepeak tank, double bottom, and hull structures around the waterline. In contrast to P1, the P2 region is characterized by denser transverse framing and a significantly stiffer structural arrangement. Compared with P1, this location exhibits a larger contact area, enabling more complex interactions between the normal and tangential force components during the collision. This condition influences the distribution of impact energy, local deformation, and the structural penetration mechanism [3].

Three collision angles 90°, 120°, and 135°, are applied at each position to represent both perpendicular and oblique collision scenarios that commonly occur during shipping operations, as illustrated more clearly in Figure 3. The 90° case serves as the reference condition for a near-perpendicular impact, whereas the 120° and 135° cases represent oblique scenarios in which the tangential force component progressively dominates. Previous studies have shown that variations in the collision angle influence the energy-transfer mechanism, the crushing-force distribution, and the deformation pattern of the ship structure [3,6]. A constant velocity of 5 m/s is maintained across all scenarios to ensure that the observed differences in structural response are primarily attributable to variations in collision position and angle.

Table 3. Simulation Scenario Matrix

Collision Position	**Collision Angle**	**Initial Velocity**
P1 – Main Deck	90°	5 m/s
P1 – Main Deck	120°	5 m/s
P1 – Main Deck	135°	5 m/s
P2 – Mid-Body (Bulbous Bow)	90°	5 m/s
P2 – Mid-Body (Bulbous Bow)	120°	5 m/s
P2 – Mid-Body (Bulbous Bow)	135°	5 m/s

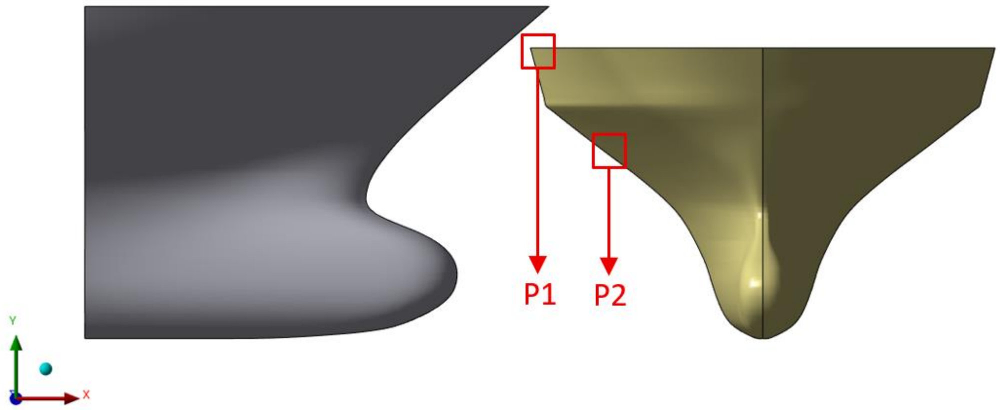

Figure 2. Collision positions on the LPG carrier hull: (P1) main deck / upper shoulder region, (P2) mid-body / mid-bulbous bow region

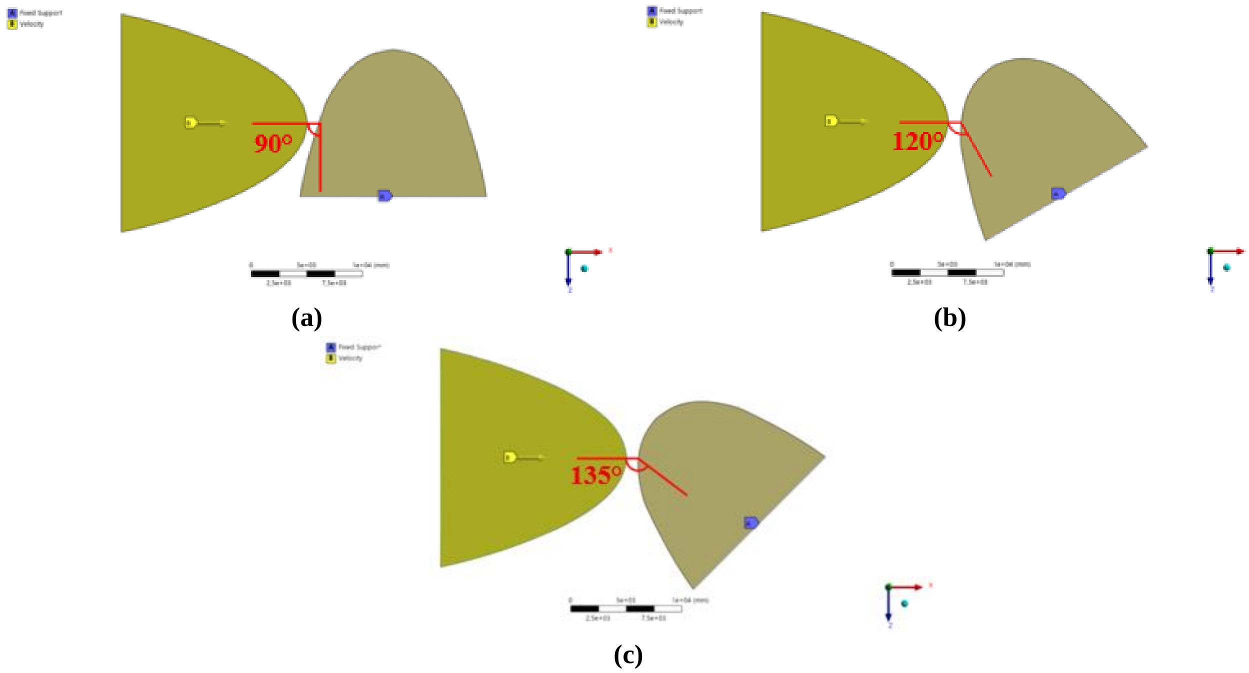

Figure 3. Collision angle configurations: (a) 90°, (b) 120°, (c) 135°

2.3. *Formulation and Approach*

The Explicit Dynamic finite element analysis adopted in this study evaluates three principal structural response quantities: directional displacement, crushing force, and internal energy. The fundamental formulations underlying each of these quantities are presented below.

2.3.1 *Directional Displacement*

Directional displacement is the displacement of a point on the ship structure in a specified direction as a result of the collision load. In the context of ship collision, the directional displacement is measured along the direction of impact (the global X-axis in ANSYS) in order to determine how far the striking bow penetrates into the hull of the struck ship. In its simplest form, the directional displacement is expressed as the difference between the final and initial positions of a point on the structure:

$$\delta = u(t) - u(0) \tag{1}$$

where δ is the directional displacement (m), $u(t)$ is the position of the point at time t under the collision load (m), and $u(0)$ is the initial position of the point prior to collision (m). The maximum value, δ_max, recorded throughout the simulation represents the maximum penetration depth of the bow into the side shell and is extracted directly from the Directional Deformation output in ANSYS.

2.3.2 *Crushing Force*

The crushing force is the force that develops at the contact surface between the striking bow and the hull plating of the struck ship during the collision process. This force is the principal indicator of structural resistance and is used to construct the crushing force–displacement curve ($F - \delta$). In Explicit Dynamic finite element analysis, the crushing force at each time step is obtained directly as the total reaction force at the contact surface between the bow and the hull plating, and can be expressed simply as:

$$F = F_{reaction} \tag{2}$$

where F is the crushing force (N), and $F_{reaction}$ is the total reaction force at the contact surface, extracted directly from the Force Reaction output of the ANSYS Explicit Dynamic solver. The value of F is subsequently plotted against the directional displacement δ (Equation 1) at each time step to construct the crushing force–displacement curve ($F - \delta$). The peak value of the $F - \delta$ curve, F_{max}, represents the maximum crushing force that the structure is capable of withstanding before progressive plastic collapse occurs. Physically, F_{max} is reached when the stress in the material at the contact zone exceeds the yield stress σy = 285 MPa (Table 2) over a significant contact area, leading to extensive plastic deformation and a consequent reduction in the local structural stiffness.

2.3.3 Internal Energy

Internal energy is the energy absorbed by the struck ship structure through plastic deformation during the collision. The greater the internal energy absorbed, the greater the capacity of the structure to attenuate the collision energy, thereby reducing the risk of hull failure. Physically, the internal energy is equivalent to the area under the crushing force–displacement curve (F–δ), expressed as:

$$E_{int} = \int F \cdot d\delta \quad (3)$$

where E_{int} is the absorbed internal energy (J), F is the crushing force at each stage of deformation (N), and $d\delta$ is the incremental directional displacement (m). This equation indicates that the larger the area under the $F - \delta$ curve, the greater the energy dissipated by the structure through plastic deformation.

The energy converted into internal energy originates from the initial kinetic energy of the striking ship, which is calculated in its simplest form as:

$$E_k = \frac{1}{2} m v^2 \quad (4)$$

where E_k is the kinetic energy of the striking ship (J), m is the mass of the ferry as listed in Table 1 (kg), and v is the initial collision velocity of 5 m/s. This initial kinetic energy constitutes the energy available for conversion into internal energy during the plastic deformation process.

Throughout the simulation, the total system energy is monitored via the energy balance of the Explicit Dynamic solver, comprising the kinetic energy and the internal energy:

$$E_{total} = E_k + E_{int} \quad (5)$$

where E_{total} is the total system energy (J). During the collision, a portion of E_k of the striking ship is converted into E_{int} within the struck structure. In this study, the value of E_{int} is extracted directly from the Internal Energy output in ANSYS for each simulation scenario and is adopted as the principal crashworthiness indicator of the structure.

2.4. Simulation Settings and Boundary Conditions

The LS-DYNA solver within ANSYS Workbench 2024 R2 is utilized for all simulations, employing an explicit time-integration scheme to efficiently capture short-duration, highly nonlinear collision events. The solver automatically controls the time step to maintain numerical stability throughout the simulation. Frictional contact between the bow surface and the side-shell plating is modeled using a Coulomb friction coefficient of μ = 0.3, which is representative of wet steel on steel contact [11].

For the boundary conditions, the struck LPG carrier is fully constrained using a Fixed Support (Point A), representing a berthed or moored condition typical of port and inter-island collision scenarios. An initial velocity of 5 m/s is applied to the striking ferry bow via a Velocity condition (Point B) along the direction of impact. The direction of impact is defined by the collision angle θ relative to the side shell of the struck ship. As the oblique angle increases, the proportion of the tangential force component increases, while the normal force component responsible for direct penetration into the hull decreases. These boundary conditions are illustrated in Figure 4.

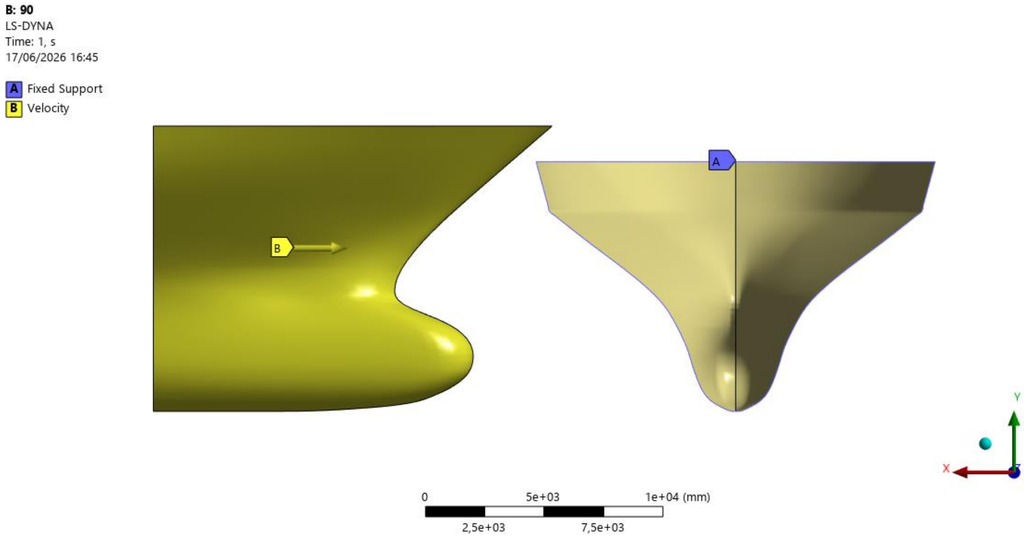

Figure 4. Boundary conditions of the explicit dynamic simulation

All six simulation scenarios in Table 3 utilize identical boundary conditions and material properties, as well as a uniform mesh size of 100 mm. The choice of a 100 mm mesh size is based on the model's hull plate thickness of 15 mm, yielding an ELT ratio of 100/15 = 6.67. This ratio falls within the recommended ELT range of 4–10 [21], supporting the selection of a 100 mm mesh, consistent with the benchmarking study. The application of a 100 mm mesh in the full-scale ship collision simulation also aligns with meshing practices previously reported for double-hull ship collision simulations [22]. The uniformity of simulation conditions ensures that observed differences in output quantities directional displacement, crushing force, and internal energy are attributable solely to variations in collision position and angle.

The hull surfaces of both vessels are meshed in ANSYS Workbench with linear quadrilateral shell elements, while triangular elements are limited to sharply curved regions such as the bulbous bow. Mesh defeaturing (10 mm) and a high smoothing level are applied to maintain uniform element quality at the P1 and P2 collision zones. The resulting full-scale mesh contains 121,743 nodes and 122,188 elements, as shown in Figure 5.

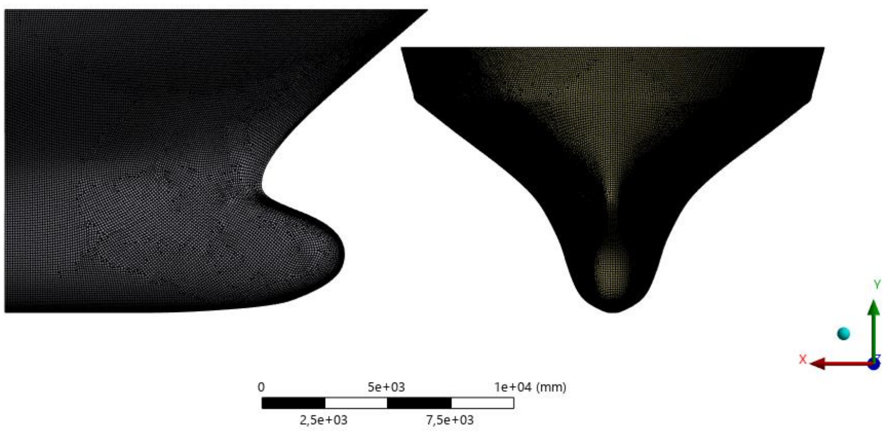

Figure 5. Finite element mesh of the full-scale ship models

2.5. Validation and Benchmarking Study

A benchmarking study was conducted to verify the accuracy of the numerical model by comparing simulation results with quasi-static penetration experimental data reported in the literature [10]. The validation specimen was an unstiffened plate of S235JR-EN10025 steel measuring 1200 × 720 × 5 mm, penetrated by a conical indenter with a spherical tip (tip radius of 200 mm, apex angle of 90°), with the plate fully constrained on all four edges and the indenter treated as a rigid body. The applied impact indenter velocity was 1.67 m/s, in accordance with the experimental test conditions adopted in a recent double-hull evaluation study [22]. The simulation was performed using nonlinear FEM in ANSYS to represent the quasi-static penetration condition.

Three mesh sizes were evaluated: 10, 20, and 30 mm. The model accuracy was assessed by comparing the crushing force–displacement curves against the experimental reference [10]. The mesh selection was guided by the Element Length-to-Thickness (ELT) ratio criterion; for a plate thickness of 5 mm, the recommended ELT range of 4–10 [21] corresponds to mesh sizes of 20–50 mm. The complete benchmarking results are presented in Table 4. The results demonstrate a clear trend among the evaluated mesh sizes: the intermediate mesh size yields the best agreement with the experimental reference. The 10 mm mesh, with an ELT ratio of 2 falling below the recommended range, produces a relatively high force error of 9.94% and a displacement error of 5.87%, indicating that overly fine discretization in this configuration does not necessarily improve accuracy and may introduce numerical artifacts associated with element distortion during large plastic deformation. The 20 mm mesh (ELT = 4), positioned at the lower bound of the recommended ELT range, achieves the lowest force error of 1.07% and displacement error of 2.28%, confirming it as the optimal configuration among the mesh sizes evaluated. The 30 mm mesh (ELT = 6), while still within the recommended ELT boundary, shows an increase in force error to 4.06% and displacement error of 2.15%, suggesting that coarser discretization begins to underrepresent the local deformation field.

Table 4. Benchmarking Results: Present Study vs. Experimental Data [10]

Mesh (mm)	**Present Study**		**Experimental Data [10]**		**Disp. Error (%)**	**Force Error (%)**
	Displacement (mm)	Force (kN)	Displacement (mm)	Force (kN)		
10	188.25	1350.9	200	1500	5.87	9.94
20	195.43	1484	200	1500	2.28	1.07
30	204.31	1561	200	1500	2.15	4.06

Based on the systematic evaluation summarized in Table 4, the 20 mm mesh is selected as the reference configuration. The complete comparison of force–displacement curves across all mesh sizes with the experimental reference and the prior simulation [20] is shown more clearly in Figure 6. Overall, all mesh variants capture the initial linear-elastic stiffness with good fidelity, as evidenced by the near-coincident ascending branches up to approximately 190 mm of displacement. The divergence between curves becomes apparent in the post-peak regime, where element erosion and plate tearing govern the structural response. The experimental curve exhibits a gradual drop in force following the peak at approximately 200 mm of displacement, reflecting the progressive nature of plate tearing in the physical specimen. The previous simulation [20] shows a steeper post-peak descent, while the present 20 mm mesh result closely follows the experimental trajectory through both the peak force and the subsequent softening phase. The 10 mm mesh notably produces a premature peak and an abrupt post-peak drop, consistent with its relatively higher force error reported in Table 4. The 20 mm mesh curve aligns most closely with the experimental reference across the entire displacement range, validating the selected mesh configuration for use in the full-scale ship collision model.

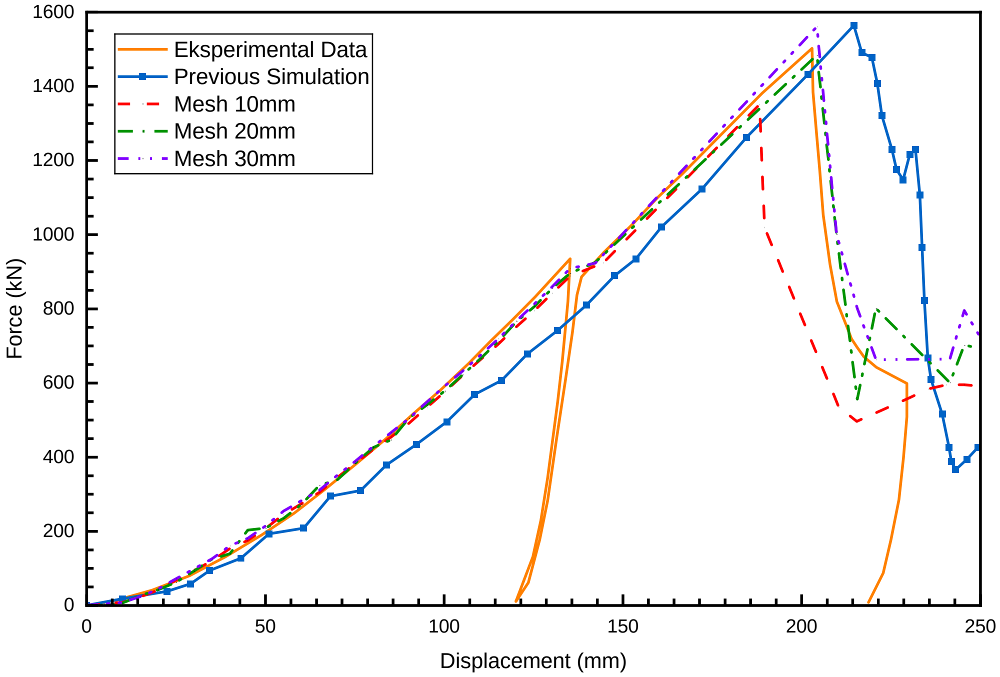

Figure 6. Comparison of crushing force–displacement curves: Experimental data [10], Previous simulation [20], Results of the present study.

As an additional comparison, a previous numerical study [20] on the same plate specimen employed a 20 mm mesh and reported a crushing force error of 4.04% relative to the reference experimental data [10]. The simulation results obtained in the present study using a 20 mm mesh show good agreement with both the experimental data and the prior simulation [20], with a force error of 1.07%, notably lower than the 4.04% error reported by [20]. This comparison indicates that the modeling procedure adopted in the present study achieves accuracy comparable to or better than that of previously published similar studies. The deformation pattern and equivalent plastic strain distribution at the maximum penetration depth across all three references are shown more clearly in Figure 7. In the experimental result (a), the deformed plate exhibits a characteristic circular dome shape centered on the indenter contact zone, with visible tearing initiating at the periphery of the contact area, a failure mode consistent with membrane stretching followed by localized fracture. The previous simulation (b) reproduces the general dome morphology, though the strain contour appears more concentrated, with a sharper transition between the high-strain central zone and the surrounding low-strain region. The present simulation (c) shows notably improved agreement with the experimental deformation profile: the equivalent plastic strain contour is more smoothly distributed, the dome geometry is broader and more consistent with the physical specimen, and the maximum strain is spatially located at the contact perimeter rather than directly at the indenter tip, a pattern that aligns with the tearing initiation mechanism observed experimentally. The color gradient from red (maximum strain) to blue (zero strain) in (c) confirms that plastic work is distributed across a realistic structural volume, thereby validating the material model, boundary conditions, and mesh configuration adopted in this study.

(a)

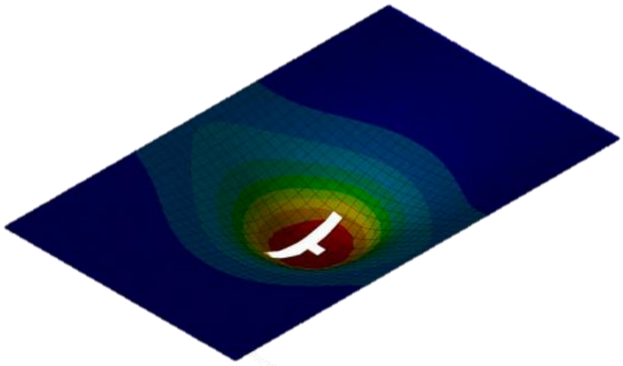

(b)

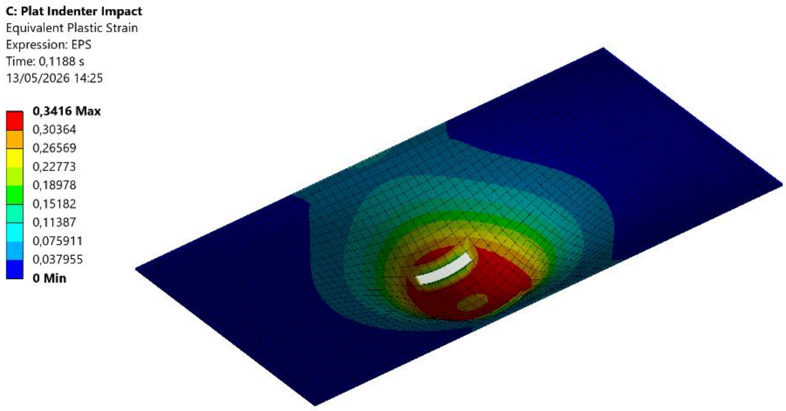

(c)

Figure 7. Comparison of deformation and plastic strain at maximum penetration: (a) Experimental results [10], ((b) Simulation of [20] at 20 mm mesh, (c) Present simulation at 20 mm mesh

It should be noted that the 20 mm mesh optimized in the benchmarking study applies to a thin 5 mm laboratory-scale plate specimen, whereas the full-scale ship collision simulation employs a 100 mm mesh, yielding an ELT ratio of 6.67 relative to the 15 mm hull plate thickness, still within the recommended range [21]. The modeling procedure, the S235JR-EN10025 material properties, the boundary conditions, and the contact settings validated through the benchmarking study are therefore confirmed to be valid and can be reliably adopted as the basis for subsequent ship collision simulations.

3. Results and Discussion

This section presents the simulation results of oblique bow collision for six scenarios combining collision position (P1: main deck; P2: mid-body / bulbous bow region) and collision angle (90°, 120°, 135°) under a constant initial velocity of 5 m/s. Three structural response quantities are evaluated sequentially: directional displacement in Subsection 3.1, crushing force in Subsection 3.2, and internal energy in Subsection 3.3. A summary of the peak values of the three quantities for all scenarios is presented in Table 5 as a reference for the discussion.

Table 5. Summary of Peak Simulation Results for All Collision Position (v = 5 m/s)

Collision Position	Crushing Force (MN)	Displacement (m)	Internal Energy (MJ)
P1 – 90°	18.73	1.39	9.42
P1 – 120°	13.72	1.38	8.88
P1 – 135°	8.41	1.49	8.86
P2 – 90°	31.44	1.10	7.77
P2 – 120°	30.18	1.34	9.85
P2 – 135°	29.14	1.39	9.61

3.1 Effect of Collision Angle Variation on Structural Deformation

The simulation results show that the variation in collision angle significantly affects the pattern and spatial extent of plastic deformation in the struck hull. At both P1 and P2, the largest deformation is concentrated in the zone of direct contact between the striking bow and the side-shell plating of the struck ship. As shown in Figures 8 and 9, a collision angle of 90° produces deformation that is more localized at the point of impact, whereas at 120° and 135°, the deformation zone extends along the side-shell plating. This behavior reflects the fact that an increase in collision angle enlarges the tangential force component, distributing the collision energy over a larger structural area rather than concentrating it at a single penetration point.

In addition, changes in the collision angle also affect the dominant damage mechanism. At 90°, bow penetration produces deeper plastic deformation due to the dominance of the normal force component, which drives membrane stretching of the outer plate. At 135°, shear deformation becomes more dominant, reducing the penetration depth while extending the longitudinal damage range of the hull. This phenomenon is consistent with previous analytical studies [4, 5], which reported that an increase in the oblique angle shifts the failure mechanism from localized tearing to distributed shear deformation and reduces the concentration of crushing force at the point of impact.

The comparison between P1 and P2 in Figures 8 and 9 also reveals differences in the deformed area that are consistent with the differences in plate thickness and framing configuration at the two positions. At P1, the deformation tends to form a sharp indentation with a steep gradient, owing to the relatively thin deck plating and the limited supporting structure. At P2, the deformation is distributed over a larger area but with a more controlled penetration depth, indicating that the denser transverse framing in the mid-body region helps distribute the deformation load to the surrounding structural elements.

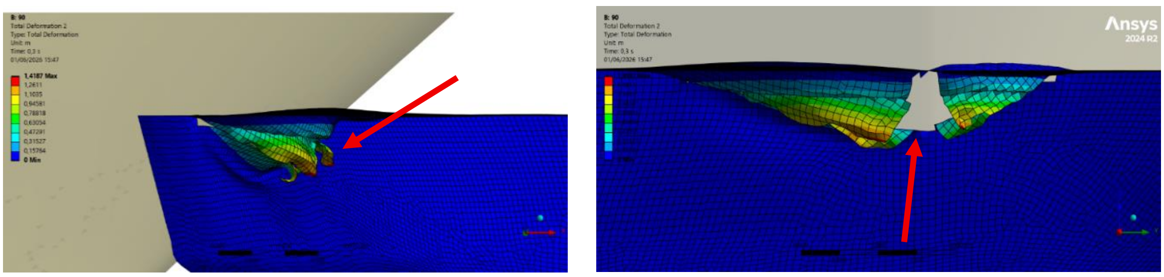

(a)

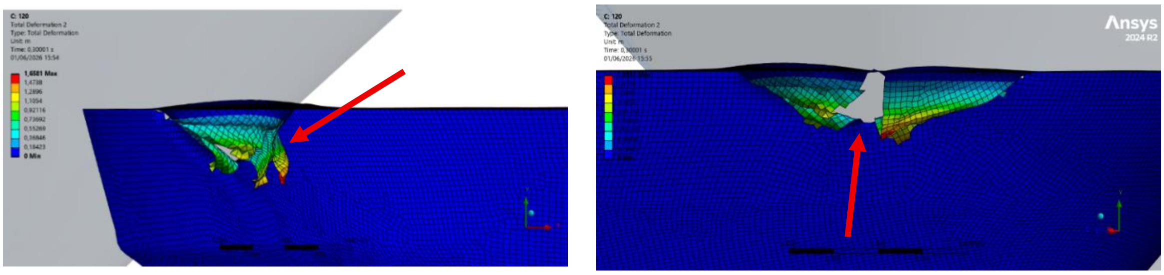

(b)

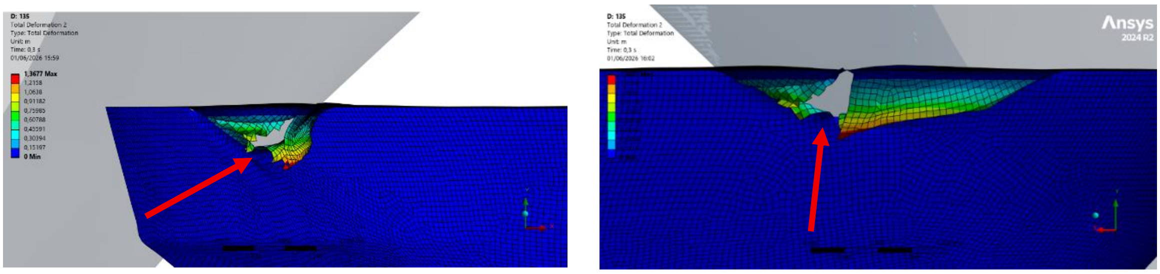

(c)

Figure 8. Deformation contours at collision position P1 (main deck): (a) 90°, (b) 120°, (c) 135°

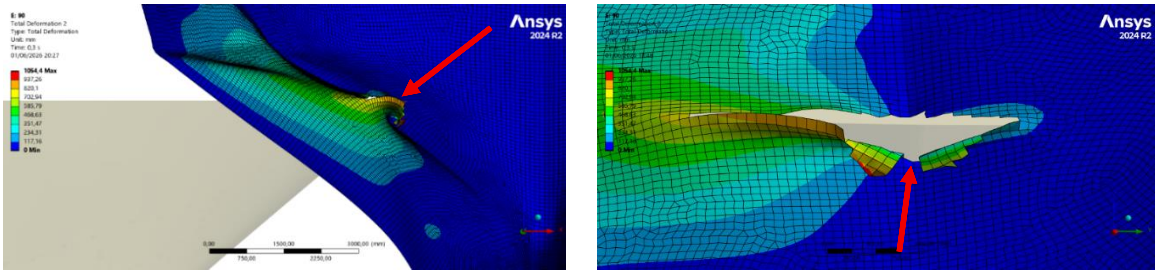

(a)

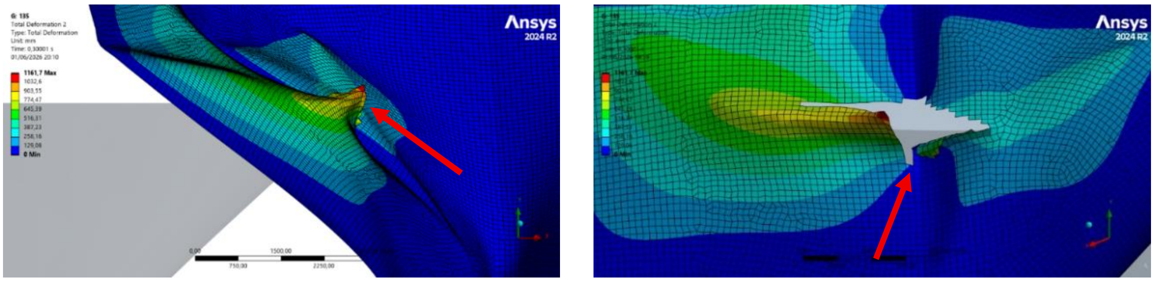

(b)

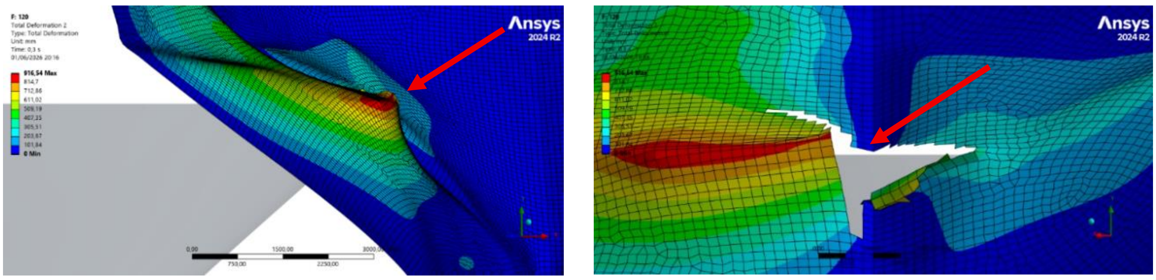

(c)

Figure 9. Deformation contours at collision position P2 (mid-body): (a) 90°, (b) 120°, (c) 135°

3.2 Crushing Force Analysis (Force–Displacement Response)

The crushing force–displacement curves (Figure 10) show that the ship's structural response is strongly influenced by both the collision position and the collision angle. A direct visual inspection of the combined plot immediately reveals two distinct curve clusters, clearly separating the structural response of the main deck (P1) from the mid-body (P2). In all variants, the crushing force increases with displacement during the elastic phase until it reaches a maximum value, after which it fluctuates due to progressive plastic deformation and local structural collapse. The peak crushing force and the displacement at peak force for all scenarios have been summarised in Table 5.

At collision position P1 (main deck), the peak crushing force decreases monotonically with increasing collision angle. The P1-90° variant produces a maximum crushing force of 18.73 MN, which decreases to 13.72 MN at P1-120° and further to 8.41 MN at P1-135°. This systematic decrease reflects the reduction in the normal force component as the oblique angle increases; a larger collision angle results in a smaller force component acting perpendicular to the hull, thereby reducing local penetration. The main deck region (P1) has relatively thin outer plating with limited transverse framing support, resulting in lower overall resistance—consistent with the more localized deformation pattern shown in Figure 8.

In contrast, collision position P2 (mid-body / bulbous bow region) produces a substantially higher peak crushing force: 31.44 MN at P2-90°, 30.18 MN at P2-120°, and 29.14 MN at P2-135°. As observed in the upper cluster of the graph, the relatively small inter-angle variation at P2 ($\Delta F \approx 2.3$ MN) compared with P1 ($\Delta F \approx 10.3$ MN) indicates that the denser transverse framing in the mid-body region provides a stiffness-based resistance that is relatively insensitive to the angle of impact. The dominant finding is that the collision position has a more decisive influence on the magnitude of the peak crushing force than the collision angle: the P2-to-P1 crushing force ratio exceeds 1.6 at 90°, confirming that the local structural topology frame spacing, plate thickness, and web depth are the principal determining factors of the crushing force.

Furthermore, Table 5 reveals a critical behavioral difference based on the impact angle at position P2. The P2-90° variant achieves the highest peak crushing force (31.44 MN) relatively early at a displacement of 1.10 m. Conversely, under oblique impact conditions, the structures reach their peak resistance at deeper penetrations (1.34 m for 120° and 1.39 m for 135°). This earlier peak at 90° indicates that, while the dense transverse framing provides high initial stiffness against perpendicular impacts, it undergoes a more abrupt local collapse than the gradual energy dissipation observed in oblique scenarios.

The curves in Figure 10 also provide additional insight into the structure's failure behavior. The P1 curves in the lower cluster exhibit highly fluctuating patterns and tend to be more gradual, continuing to increase without reaching a sharp peak. This prolonged fluctuation indicates that the structure at P1 has not completely collapsed within the simulated displacement range. In contrast, the P2 curves exhibit a clear elastic–plastic phase, followed by a distinct force peak and a softening phase, reflecting progressive local collapse of the framing and plating around the contact zone. The difference in the curves' behavior reinforces the conclusion that P2 reaches a more severe structural damage condition than P1 within the same velocity and displacement range.

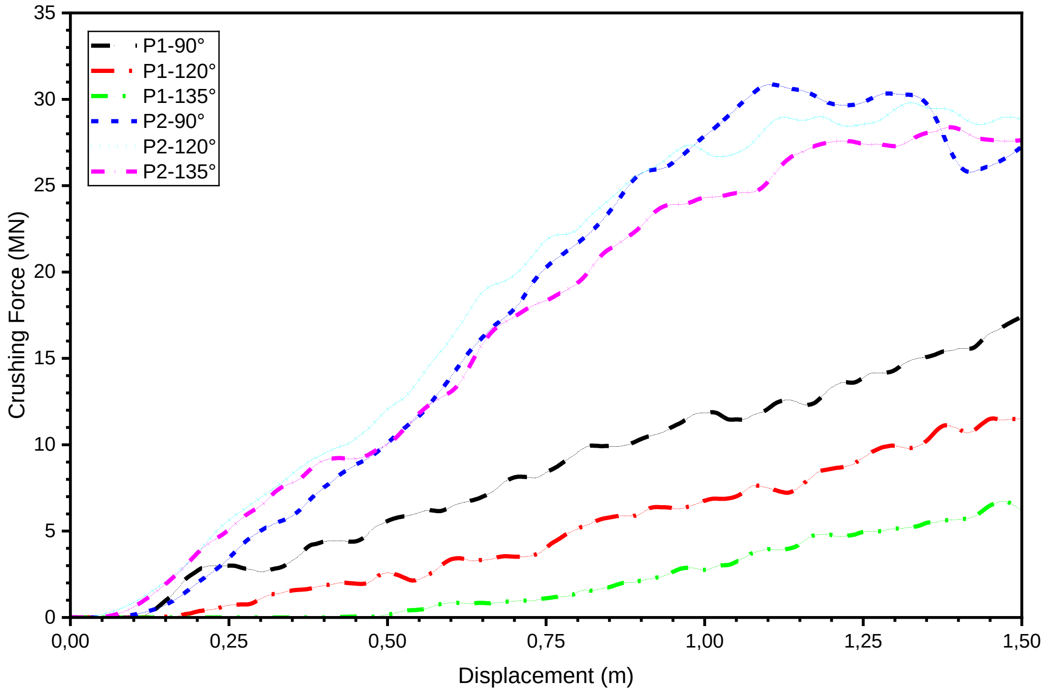

Figure 10. Comparison of crushing force–displacement curves for all collision scenarios

3.3 Internal Energy Absorption Analysis

Internal energy (Equation 3) is used to evaluate the capacity of the structure to absorb collision energy through plastic deformation. The greater the internal energy absorbed, the greater the crashworthiness of the structure and its ability to reduce the risk of catastrophic hull failure.

The simulation results (Table 5) show that the maximum internal energy at position P1 ranges from 8.86 to 9.42 MJ, as illustrated by the internal energy absorption time histories in Figure 11. The highest value occurs at P1-90° (9.42 MJ) and the lowest at P1-135° (8.86 MJ). This narrow variation ($\Delta \approx 6\%$) indicates that the thin plating in the P1 region approaches its ductility limit across all angle cases, such that the plastic energy absorption capacity is saturated regardless of the force direction—consistent with the continuously increasing crushing force pattern without a sharp peak observed in Figure 10.

At position P2, a markedly different pattern is observed. The highest internal energy occurs at P2-120° (9.85 MJ), followed by P2-135° (9.61 MJ) and P2-90° (7.77 MJ). This counter-intuitive result in which the case with the highest peak crushing force (P2-90°) does not yield the highest energy absorption is explained by the geometry of the impact path. The perpendicular impact at P2 concentrates deformation within a small but deep penetration zone (visible in Figure 9a), rapidly exhausting local ductility and triggering element erosion, thereby limiting the total area under the $F - \delta$ curve that contributes to energy absorption (Equation 3). At angles of 120° and 135°, the oblique contact path distributes the deformation over a longer segment of the hull (Figures 9b and 9c), engaging additional framing and plating in plastic work and resulting in a higher cumulative energy absorption. This finding is consistent with previous observations [3,15] that an oblique contact path distributes energy over a wider structural region.

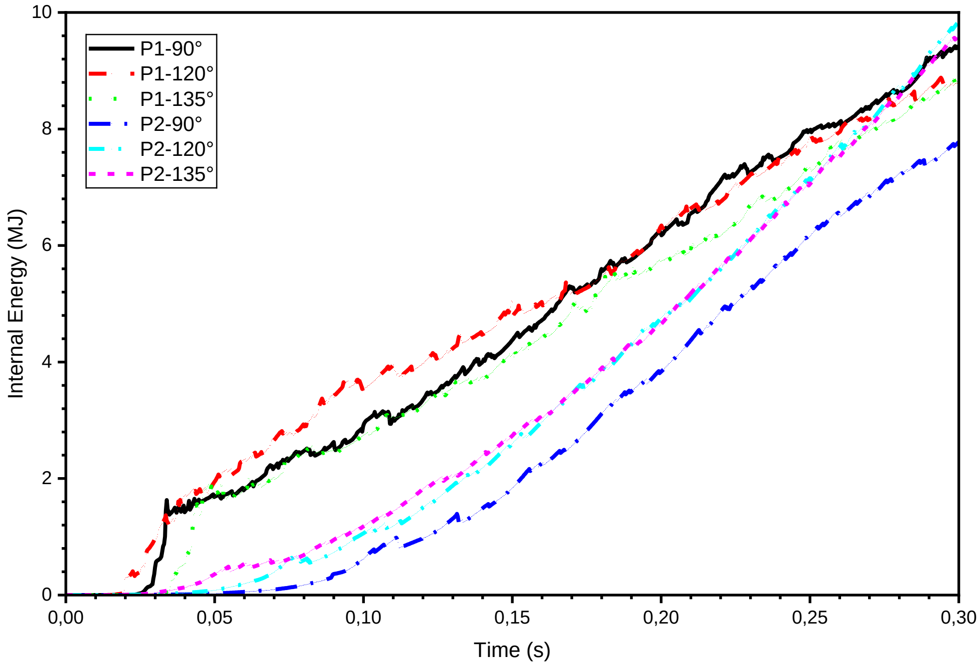

Figure 11. Internal energy absorption time histories curves

Overall, the results from the three subsections demonstrate a consistent relationship: position P2 produces a substantially higher crushing force than P1, yet its energy absorption efficiency varies more strongly with the collision angle. The P2-120° variant exhibits the best crashworthiness performance among the six scenarios, achieving both high structural resistance and maximum energy dissipation, whereas P2-90° despite producing the highest overall peak crushing force—represents the case with the lowest energy absorption at position P2. This finding reinforces the principle that structural safety evaluation cannot rely solely on peak crushing force but must also consider internal energy absorption capacity as an equally important safety metric [6,7,18]. Notably, although all six scenarios exhibit substantial plastic deformation within the contact zone, none of the force–displacement curves in Figure 10 display a sudden collapse toward zero force within the simulated displacement range, indicating that the observed structural response corresponds to progressive plastic damage rather than catastrophic structural failure. This distinction should nonetheless be interpreted with caution, as a formal assessment of hull breach or rupture would require an explicit failure criterion, such as critical strain thresholds or residual plate thickness, which lies beyond the scope of the present study.

4. Conclusion

This study conducted a systematic parametric analysis of oblique ferry-to-LPG carrier collisions using validated Explicit Dynamic FEM (LS-DYNA) at 5 m/s across six scenarios. Collision position was found to be the dominant factor governing structural resistance: the mid-body region (P2) produced a peak crushing force of 31.44 MN at 90°, over 60% higher than the main deck region (P1). Increasing the collision angle shifted the failure mechanism from concentrated bow penetration toward distributed shear deformation. Notably, peak crushing force and internal energy absorption were decoupled—the highest energy dissipation occurred at P2-120° (9.85 MJ) rather than at the highest-force case, P2-90° (7.77 MJ)—indicating that the P2-90° zone is structurally critical despite its high resistance. All scenarios exhibited progressive plastic deformation rather than catastrophic collapse, although a definitive assessment of hull breach would require a dedicated failure criterion beyond the scope of this study.

Based on these findings, three recommendations are proposed. First, berthing approach velocity and angle should be carefully managed to minimize the normal force component at the P1 deck region. Second, because the P2 zone suffers the most severe energy absorption deficit under 90° perpendicular impact, this scenario requires priority structural reinforcement, such as additional transverse framing, supporting brackets, or localized plate thickening. Third, collision safety assessments and future ship designs should treat internal energy absorption capacity and peak crushing force as equally weighted safety metrics, rather than relying on structural resistance alone. As these findings are derived under a single impact velocity and a limited set of collision positions, future studies should extend this validated numerical approach to variable collision velocities and a broader range of impact locations along the hull, supporting the development of collision-resistant ship design standards in Indonesian waters in line with Sustainable Development Goal 9 (Industry, Innovation and Infrastructure).

Acknowledgement

This research was supported by Universitas Negeri Semarang under the UNNES LPPM DPA Funds for 2026 with number: 359.8.4/UN37/PPK.11/2026. The authors would like to thank the Department of Mechanical Engineering, Faculty of Engineering, Universitas Negeri Semarang (UNNES), for supporting the computational resources and software access provided in this research.

References

[1] Sunardi, S., Nurwahyudi, A., Sulkhany, E., Setyanto, A., Supomo, H., Kertorahardjo, S.P., Safety Risk Evaluation by Vessel Type and Accident Category in an Archipelagic State: An Empirical Data Analysis from Indonesia. International Journal of Safety and Security Engineering. 2025; 15(10): p. 2103-2109.

[2] AbuBakar, A., Dow, R.S., The impact analysis characteristics of a ship's bow during collisions. Engineering Failure Analysis. 2019; 100: p. 492-511.

[3] Wang, Z., Liu, K., Chen, G., Hu, Z., An analytical method to assess the structural responses of ship side structures by raked bow under oblique collision scenarios. Proceedings of the Institution of Mechanical Engineers, Part M: Journal of Engineering for the Maritime Environment. 2021; 235(3): p. 773-791.

[4] Assaify, F.F., Zakki, A.F., Yudo, H., Analisis Dan Simulasi Kerusakan Haluan Kapal MT. Kuang 6500 DWT Akibat Tubrukan Dengan Dermaga Wharf Menggunakan Metode Element Hingga. Jurnal Teknik Perkapalan. 2022; 10(3): p. 11-20.

[5] Prabowo, A.R., Bae, D.M., Sohn, J.M., Zakki, A.F., Evaluating the Parameter Influence in the Event of a Ship Collision based on the Finite Element Approach. International Journal of Technology. 2016; 7(4): p. 592.

[6] Liu, B., Villavicencio, R., Pedersen, P.T., Soares, C.G., Analysis of structural crashworthiness of double-hull ships in collision and grounding. Marine Structures. 2021; 76: p. 102898.

[7] Ringsberg, J.W., Amdahl, J., Chen, B.Q., Cho, S.R., Ehlers, S., Hu, Z., et al., MARSTRUCT benchmark study on nonlinear FE simulation of an experiment of an indenter impact with a ship side-shell structure. Marine Structures. 2018; 59: p. 142-157.

[8] Bahatmaka, A., Kim, D.J., Samuel, S., Prabowo, A.R., Zaw, M.T., Investigation on the performance of the traditional Indonesian fishing vessel. Proceeding of the 4th International Conference on Mechanical Engineering (ICOME 2017); 2017; Surabaya, Indonesia. EDP Sciences (MATEC Web of Conferences); 2018. 159. p. 02056.

[9] Fahmi, F.F., Bahatmaka, A., Naryanto, R.F., Won, L.S., Numerical Analysis of The Effect of Chine Variation on The Design of The Senopati Catamaran Fishing Boat on Resistance Based on Maxsurf Resistance Software. Jurnal Inovasi Mesin. 2026; 7(2): p. 24-33.

[10] Alsos, H.S., Amdahl, J., On the resistance to penetration of stiffened plates, Part I – Experiments. International Journal of Impact Engineering. 2009; 36(6): p. 799-807.

[11] Prabowo, A.R., Bae, D.M., Sohn, J.M., Zakki, A.F., Cao, B., Wang, Q., Analysis of structural behavior during collision event accounting for bow and side structure interaction. Theoretical and Applied Mechanics Letters. 2017; 7(1): p. 6-12.

[12] Prabowo, A.R., Bae, D.M., Sohn, J.M., Zakki, A.F., Cao, B., Cho, J.H., Effects of the rebounding of a striking ship on structural crashworthiness during ship-ship collision. Thin-Walled Structures. 2017; 115: p. 225-239.

[13] Prabowo, A.R., Harsritanto, B.I.R., Bae, D.M., Sohn, J.M., Bahatmaka, A., Samuel, S., Progressive structural failure of the RoRo side hull during accidental powered-bow collisions. Proceeding of the 5th International Conference on Engineering, Technology, and Industrial Application (ICETIA); 2017; Surakarta, Indonesia. AIP Publishing; 2018. 2043(1). p. 020003.

[14] Ye, X., Fan, W., Sha, Y., Hua, X., Wu, Q., Ren, Y., Fluid-structure interaction analysis of oblique ship-bridge collisions. Engineering Structures. 2023; 274: p. 115129.

[15] Zhang, Y., Yuan, Y., Zhou, J., Tang, W., A new analytical model to evaluate ship side collisions with large indentation considering interaction effects between structural components. Marine Structures. 2024; 95: p. 103596.

[16] Yi, M.S., Park, J.S., Field-Calibrated Nonlinear Finite Element Diagnosis of Localized Stern Damage from Tugboat Collision: A Measurement-Driven Forensic Approach. Journal of Marine Science and Engineering. 2025; 13(8): p. 1523.

[17] Widjaja, M.P. Numerical and Analytical Simulations of Ship-Jacket Collisions. Belgium: Université de Liège; 2016.

[18] Liu, B., Villavicencio, R., Zhang, S., Soares, C.G., Assessment of external dynamics and internal mechanics in ship collisions. Ocean Engineering. 2017; 141: p. 326-336.

[19] Rudan, S., Ćatipović, I., Berg, R., Völkner, S., Prebeg, P., Numerical study on the consequences of different ship collision modelling techniques. Ships and Offshore Structures. 2019; 14(sup1): p. 387-400.

[20] Prabowo, A.R., Ridwan, R., Tuswan, T., Smaradhana, D.F., Cao, B., Baek, S.J., Crushing resistance on the metal-based plate under impact loading: A systematic study on the indenter radius influence in grounding accident. Applications in Engineering Science. 2024; 18: p. 100177.

[21] Prabowo, A.R., Putranto, T., Sohn, J.M., Simulation of the Behavior of a Ship Hull under Grounding: Effect of Applied Element Size on Structural Crashworthiness. Journal of Marine Science and Engineering. 2019; 7(8): p. 270.

[22] Malsyage, D., Bahatmaka, A., Kirana, A.C.C, Won, L.S., Hee, S.Y., Finite Element-Based Evaluation of Double-Hull Midsection Performance under Oblique Collision. Mekanika: Majalah Ilmiah Mekanika. 2025; 24(2): p. 121-135.